

Article

Not peer-reviewed version

# Identification of New Polyacetylenes from *Dendropanax morbifera* with PPAR- $\alpha$ Activity Study

[Donglan Piao](#) , Isoo Youn , [Thanh-Hau Huynh](#) , Hyun Woo Kim , [Sang Gyun Noh](#) , [Hae Young Chung](#) , [Dong-Chan Oh](#) , [Eun Kyoung Seo](#) \*

Posted Date: 28 October 2024

doi: 10.20944/preprints202410.2138.v1

Keywords: *Dendropanax morbifera* leveille; polyacetylene; phenolic glucoside; AMP-activated protein kinase; cathepsin S; peroxisome proliferator-activated receptor



Preprints.org is a free multidisciplinary platform providing preprint service that is dedicated to making early versions of research outputs permanently available and citable. Preprints posted at Preprints.org appear in Web of Science, Crossref, Google Scholar, Scilit, Europe PMC.

Copyright: This open access article is published under a Creative Commons CC BY 4.0 license, which permit the free download, distribution, and reuse, provided that the author and preprint are cited in any reuse.

## Article

# Identification of New Polyacetylenes from *Dendropanax morbifera* with PPAR- $\alpha$ Activity Study

Donglan Piao <sup>1,†</sup>, Isoo Youn <sup>1,†</sup>, Thanh-Hau Huynh <sup>2</sup>, Hyun Woo Kim <sup>3</sup>, Sang Gyun Noh <sup>3</sup>, Hae Young Chung <sup>3</sup>, Dong-Chan Oh <sup>2</sup> and Eun Kyoung Seo <sup>1,\*</sup>

<sup>1</sup> Graduate School of Pharmaceutical Sciences, College of Pharmacy, Ewha Womans University, Seoul 03760, Republic of Korea

<sup>2</sup> Natural Products Research Institute, College of Pharmacy, Seoul National University, Seoul 08826, Republic of Korea

<sup>3</sup> Department of Pharmacy, College of Pharmacy, Pusan National University, Busan 46241, Republic of Korea

\* Correspondence: yuny@ewha.ac.kr; Te.l: +82-2-3277-3047 (E.K.S.)

† These authors contributed equally to this work.

**Abstract:** *Dendropanax morbifera* Leveille is a traditional medicine used to treat migraine headache and dysmenorrhea. In this study, a new phenolic glycoside, morbiferoside A (**1**), and three polyacetylenes, methyl (10E,9R,16R)-16-acetoxy-9-hydroxyoctadeca-10,17-dien-12,14-dienoate (**2**), methyl (10E,9R,16S)-9,16-dihydroxyoctadeca-10-en-12,14-dienoate (**3**), and methyl (10Z,9R,16S)-9,16-dihydroxyoctadeca-10,17-dien-12,14-dienoate (**4**), were isolated from the aerial parts of *D. morbifera*, together with seven known compounds (**5**–**11**). Importantly, the isolates, **7** and **9** were found in the family Araliaceae for the first time in this study. Compounds **1**–**11** were evaluated for their binding affinity to AMPK and CTSS receptors using *in silico* docking simulations. Only compound **8** increased the protein expression levels of PPAR- $\alpha$ , Sirt1, and AMPK when administered to HepG2 cells as a PPAR- $\alpha$  agonist. On the other hand, **8** did not produce any significant reduction in CTSS activity. This study could pave the way for the discovery of novel treatments from *D. morbifera* targeting PPAR- $\alpha$  and AMPK.

**Keywords:** *Dendropanax morbifera* leveille; polyacetylene; phenolic glucoside; AMP-activated protein kinase; cathepsin S; peroxisome proliferator-activated receptor

## 1. Introduction

*Dendropanax morbifera* Leveille belongs to the family Araliaceae and is an endemic species in Korea [1]. *D. morbifera* is an evergreen tree with a golden color, medium size (height of about 15 meters), and leaves resembling duck palms [2]. The name of this plant, which is commonly known as Hwangchil in Korea, originates from *Hwang* meaning golden yellow and *chil* meaning coatings because it has been used as a natural golden coating. *D. morbifera* is a traditional medicine commonly used to treat migraine headache, dysmenorrhea, and rheumatoid arthritis [3]. In addition, *D. morbifera* has been reported to exhibit wide biological activities, such as anti-diabetic [4], anti-cardiac hypertrophy [5], cytotoxic [6], and anti-inflammatory properties [7].

More than 90 compounds have been identified in *D. morbifera*, including phenylpropanoids, flavonoids, and polyacetylenes [8]. Phenylpropanoids are secondary metabolites found in various plants, primarily synthesized through the shikimate pathway [9]. Enzymes such as oxygenases, ligases, and oxidoreductases ultimately generate a diverse array of phenylpropanoid compounds that exhibit cytotoxic [10], anti-oxidant [11], and anti-inflammatory activities [12]. Flavonoids are synthesized via two pathways: the shikimate pathway to produce the phenylpropanoid skeleton and the acetate pathway to provide 2-carbon unit building blocks [13]. They exhibit activities beneficial for treating cytotoxic conditions [14], cardiovascular disease [15], and metabolic disease [16]. Polyacetylenes are typically unstable compounds with a unique carbon–carbon triple bond structure. Due to their extensive biological activity and novel biosynthetic pathways, these compounds have

attracted considerable attention [17,18]. Isotope tracing studies indicated that most polyacetylenes originate from precursors of fatty acids and polyketides [17]. This class of the compounds has demonstrated efficacy in treating diabetes [19] and inflammation [20].

As nutritional supports and life expectancy grow, metabolic syndromes, such as T2 diabetes mellitus, hyperlipidemia, and cardiac diseases, are becoming more prevalent and now occur in nearly 25% of the adult population worldwide [21]. Although diet and exercise are the primary treatments for those diseases, pharmaceutical therapy is necessary to relieve severe obesity, dyslipidemia, diabetes, and hypertension. Current treatments, including glucagon-like peptide-1 agonists, insulin sensitizers, sodium glucose transporter-2 inhibitors, antiplatelet agents, HMG-CoA reductase inhibitors, and renin-angiotensin system blockers, are administered to control those diseases in patients. However, long-term use of those drugs and severe side effects burden the patients who use them [22].

Peroxisome proliferator-activated receptor (PPAR-) is a transcription factor that controls various physiological processes in the body [23]. Among the three PPAR- isoforms ( $\alpha$ ,  $\beta/\delta$ , and  $\gamma$ ), PPAR- $\alpha$  is predominantly expressed in the liver, heart, and kidney and is required for fatty acid/lipoprotein metabolism and peroxisomal proliferation [24]. AMP-activated protein kinase (AMPK) is an enzyme sensor that maintains cellular energy balance [25]. Several studies have reported that PPAR- $\alpha$  activators activate the AMPK signaling pathway, thereby regulating hepatic lipogenesis, adipocyte differentiation, and glucose uptake in muscle [25–27]. Therefore, PPAR- $\alpha$  agonists can stimulate AMPK in ways favorable to the prevention of metabolic syndrome. On the other hand, cathepsin S (CTSS) belongs to the peptidase C1 family of cysteine cathepsins, which are lysosomal cysteine proteases that function in the degradation and processing of proteins [28]. CTSS is predominantly found in antigen-presenting cells such as macrophages and T cells [29], and it is stable at a neutral pH. CTSS has been found to correlate with diabetes and adipogenesis [30,31].

As mentioned above, researchers have reported that *D. morbifera* is effective against various metabolic syndromes, and AMPK and CTSS levels correlate with those diseases [32–36]. This study aims to find active ingredients from *D. morbifera* and elucidate the relationships between those compounds and AMPK, PPAR- $\alpha$ , and CTSS. Therefore, compounds were isolated, and then their structures were elucidated using NMR, HR-MS, and ECD. The biological activity of the *D. morbifera*-derived compounds was investigated by examining their effects on AMPK, PPAR- $\alpha$ , and CTSS in computer simulation and cell-based analyses.

## 2. Results and Discussion

In this study, one new phenolic glucoside (**1**) and three new polyacetylenes (**2–4**) were isolated from the aerial parts of *D. morbifera*, together with seven known compounds (**5–11**). The known compounds were identified as methyl (10*E*,9*R*,16*S*)-9,16-dihydroxyoctadeca-10,17-dien-12,14-dienoate (**5**) [37], syringin (**6**) [38], syringinoside (**7**) [38], hyperoside (**8**) [39], koaburside (**9**) [40], epifriedelanol (**10**) [41], and dihydroconiferyl ferulate (**11**) [42]. Importantly, **7** and **9** were reported for the first time in the family Araliaceae. According to previous research, **5** significantly inhibits melanin production [37]. Compound **6** possesses anti-inflammatory [43], cytotoxic [44], and immunomodulatory properties [45]. **7** was found in *Wikstroemia sikokiana* in 1988 [38], and it has also been isolated from other plants, such as *Stelleropsis iranica* and *Daphne oleoides* [46,47]. **8** has been studied extensively for its various biological activities, including anti-inflammatory [48], antidepressant-like [49], and antibacterial effects [50]. **9** has been isolated from *Betula platyphylla* and *Walsura robusta* [51,52] and shown antioxidant activity [52]. **10** has been reported to have anti-aging effects [53], as well as antibacterial and anti-tumor properties [54,55]. **11** can be used as a cancer stem cell inhibitor for the treatment of breast cancer [6].

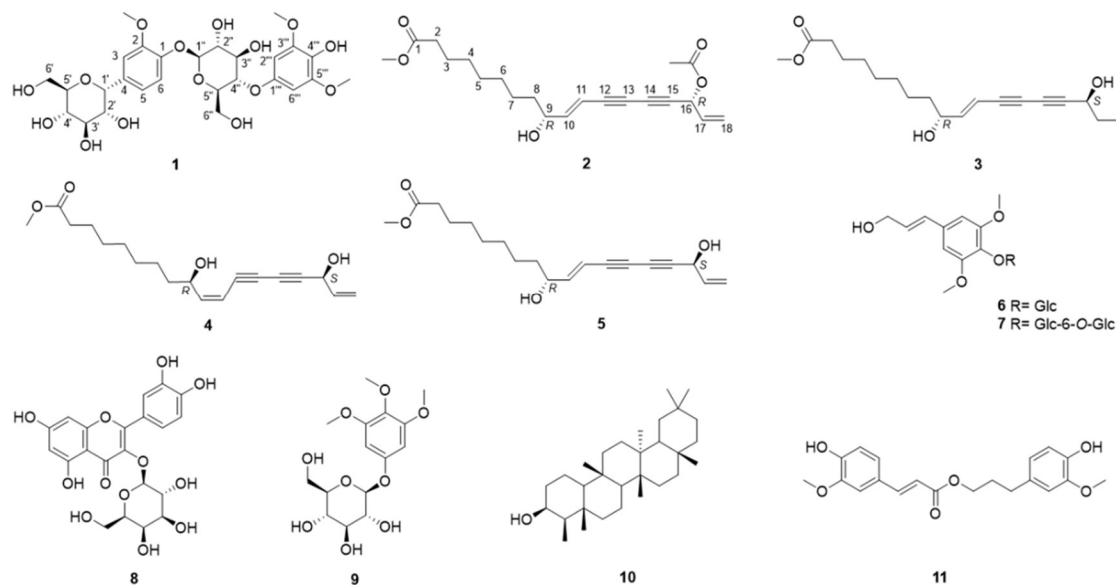


**Figure 1.** The structures of compounds 1–11.

### 2.1. Structure Elucidation

Compound **1**, a yellow amorphous solid, revealed a molecular ion peak at  $m/z$  601.2136  $[M + H]^+$  in the HRESIMS, which gave rise to the molecular formula  $C_{27}H_{37}O_{15}$ . The  $^1H$  NMR spectrum of **1** showed three methoxy signals at  $\delta_H$  3.85 (3H, s) and 3.82 (6H, s), 1,2-disubstituted benzenyl protons at  $\delta_H$  7.11 (1H, dd,  $J = 8.4, 1.4$  Hz, H-6), 7.08 (1H, m, H-3), and 6.90 (1H, dd,  $J = 8.4, 2.0$  Hz, H-5), and a 1,2,3-trisubstituted aromatic system from the signals at  $\delta_H$  6.73 (2H, s, H-2''' and 6''') (Table 1). Furthermore, the anomeric protons of two sugar moieties were observed at  $\delta_H$  4.95 (1H, d,  $J = 5.3$  Hz)/ $\delta_C$  73.8 (C-1') and 4.88 (1H, d,  $J = 7.6$  Hz)/102.9 (C-1''), indicating the presence of C- $\alpha$ -glucoside and O- $\beta$ -glucoside moieties [56–58]. The  $^{13}C$  NMR spectrum showed 27 carbon resonances: 12 carbons for two aromatic systems ( $\delta_C$  147.2, 150.5, 112.4, 137.5, 120.8, 117.6, 139.9, 105.2, 154.3, 135.9, and 105.2), 12 carbons for two sugar moieties ( $\delta_C$  73.8, 87.2, 71.4, 78.2, 61.5, 62.6, 102.9, 75.0, 77.9, 75.2, 77.4, and 64.3), and 3 carbons for methoxy groups ( $\delta_C$  56.8 and 56.7) (Table 1). The assignments of the methoxy groups were supported by the correlations between  $\delta_H$  3.85/C-2, 3.82/C-3''' and C-5''' in the HMBC spectrum, thus positioning them at C-2, C-3''', and C-5'''. By comparing the  $^1H$  and  $^{13}C$  NMR spectra, it was determined that the phenyl glucoside moiety is nearly identical to that of 2-methoxyphenyl-O- $\beta$ -D-glucopyranoside [59]. According to the HMBC correlations, H-1' shows connectivity with C-3, C-4, and C-5, indicating that the C- $\alpha$ -glucoside is attached at the H-4 position of the 2-methoxyphenyl- $\beta$ -D-glucopyranoside structure. Additionally, the HMBC correlation between H-4'' and C-1''' suggests that the phenolic moiety is attached at the H-4'' position of the 2-methoxyphenyl- $\beta$ -D-glucopyranoside structure. Although H-4'' and C-2''' are four bonds away in the compound, the HMBC correlations were observed because C-2''' and C-6''' are chemically identical, which increases peak intensity in the spectrum. The NOESY correlations observed between H-1'/H-3, H-1'/H-5, H-1''/H-6, H-4''/H-2''', and H-4''/H-6''' offered additional support regarding the position of the glucose groups in compound **1**. Overall, **1** was elucidated as a 1-O- $\beta$ -[4-O-(3,5-dimethoxy-4-hydroxyphenyl)-glucopyranosyl]-2-methoxy-4-C- $\alpha$ -glucopyranoside and named morbiferoside A. A similar phenolic diglycoside was isolated from *Heliciopsis terminalis* and analyzed for its glucose uptake stimulation effect [60]. To the best of our knowledge, this is the first report of a phenolic diglycoside isolated from *D. morbifera*.



**Table 1.** <sup>1</sup>H (400 MHz) and <sup>13</sup>C (100 MHz) NMR data for **1** in methanol-*d*<sub>4</sub>.

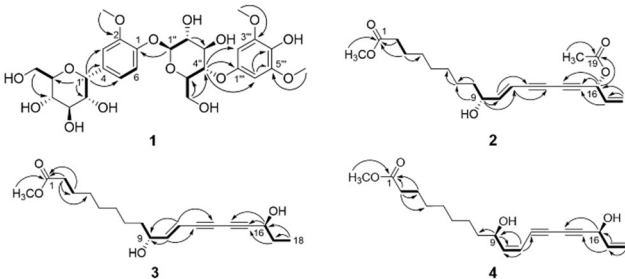
position	δ <sub>c</sub>	δ <sub>H</sub>
1	147.2	
2	150.5	
3	112.4	7.08 (1H, m)
4	137.5	
5	120.8	6.90 (1H, dd, J = 8.4, 2.0 Hz)
6	117.6	7.11 (1H, dd, J = 8.4, 1.4 Hz)
1'	73.8	4.95 (1H, d, J = 5.3 Hz)
2'	87.2	4.24 (1H, m)
3'	71.4	3.39 (1H, m)
4'	78.2	3.40 (1H, m)
5'	61.5	3.55 (1H, m)
6'	62.6	3.88 (1H, m) 3.69 (1H, m)
1''	102.9	4.88 (1H, d, J = 7.6 Hz)
2''	75.0	3.48 (1H, m)
3''	77.9	3.47 (1H, m)
4''	75.2	4.60 (1H, d, J = 5.4 Hz)
5''	77.4	3.67 (1H, m)
6''	64.3	3.54 (1H, m) 3.41 (1H, m)
1'''	139.9	
2'''	105.2	6.73 (2H, s)
3'''	154.3	
4'''	135.9	
5'''	154.3	
6'''	105.2	6.73 (2H, s)
2-OCH <sub>3</sub>	56.8	3.85 (3H, s)
3'''-OCH <sub>3</sub> /5'''-OCH <sub>3</sub>	56.7	3.82 (6H, s)

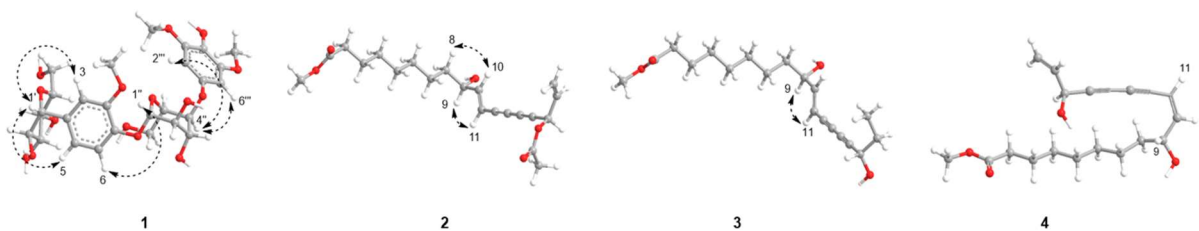
Compound **2** was obtained as a brown amorphous powder with a molecular ion peak at *m/z* 383.1835 [*M* + Na]<sup>+</sup> in the HRESIMS, showing its molecular formula as C<sub>21</sub>H<sub>28</sub>O<sub>5</sub> with 8 degrees of unsaturation. In the <sup>1</sup>H spectrum of **2** (Table 2), two sets of olefinic proton signals appeared at δ<sub>H</sub> 6.34 (1H, dd, *J* = 15.9, 5.7 Hz), 5.88 (1H, ddd, *J* = 16.9, 13.0, 5.7 Hz), 5.76 (1H, ddd, *J* = 15.9, 1.6, 0.8 Hz), 5.55 (1H, dt, *J* = 16.9, 1.1 Hz), and 5.35 (1H, dt, *J* = 10.3, 1.1 Hz) [37]. Two oxygenated methines were observed at δ<sub>H</sub> 4.20 (1H, q, *J* = 5.8 Hz)/δ<sub>C</sub> 72.0 (C-9) and 5.96 (1H, dd, *J* = 5.8, 1.0 Hz)/64.7 (C-16), together with seven methylene groups at δ<sub>H</sub> 2.30 (2H, t, *J* = 7.5 Hz,)/δ<sub>C</sub> 34.1 (C-2), 1.62 (2H, m)/24.9 (C-3), 1.31 (2H, m)/29.1 (C-4), 1.31 (2H, m)/29.0 (C-5), 1.25 (2H, s)/29.2 (C-6), 1.31 (2H, m)/25.1 (C-7), and 1.55 (2H, d, *J* = 7.2 Hz)/36.8 (C-8). The COSY correlations of **2** built the connectivity between H-2/H-3, H-8/H-9, H-9/H-10, H-10/H-11, H-16/H-17, and H-17/H-18 (Figure 2). In the HMBC spectrum of **2** (Figure 2), correlations between H-2/C-1 and H-3/C-1 established the position of a carboxyl group next to C-2, and another cross-peak from a methoxy group, (δ<sub>H</sub> 3.67) to C-1 (δ<sub>C</sub> 174.3), suggested the attachment of a methoxy group at C-1 (Figure 2). Furthermore, HMBC correlations between H-10/C-12, H-11/C-13, H-16/C-14, H-16/C-15, and H-17/C-15 indicated the existence of two consecutive acetylene functionalities (C-12 to C-15) [61]. The positions of double bonds were confirmed by the HMBC correlations from H-9 to C-10 and C-11, H-18 to C-17 and C-16, and H-17 to C-15. The Δ<sup>10,11</sup> double bond was assigned as an *E* configuration by the large coupling constant (*J*<sub>H-10/H-11</sub> = 15.9 Hz). It was also supported by NOE correlations between H-8/ H-10 and H-9/H-11.

**Table 2.** <sup>1</sup>H NMR (400 MHz) and <sup>13</sup>C NMR (100 MHz) of **2** in chloroform-*d* and **3–4** in DMSO-*d*<sub>6</sub>.

<b>2</b>		<b>3</b>		<b>4</b>	
Position	δ <sub>H</sub>	δ <sub>C</sub>	δ <sub>H</sub>	δ <sub>C</sub>	δ <sub>C</sub>
1		174.3		173.3	173.3
2	2.30 (2H, t, <i>J</i> = 7.5 Hz)	34.1	2.28 (2H, t, <i>J</i> = 7.4 Hz)	33.2	2.28 (2H, t, <i>J</i> = 7.4 Hz) 33.2
3	1.62 (2H, m)	24.9	1.50 (2H, m)	24.3	1.50 (2H, m) 24.3
4	1.31 (2H, m)	29.0 <sup>a</sup>	1.24 (2H, m)	28.3	1.25 (2H, m) 28.3
5	1.31 (2H, m)	29.1 <sup>a</sup>	1.24 (2H, m)	28.7 <sup>a</sup>	1.25 (2H, m) 28.5 <sup>a</sup>
6	1.25 (2H, m)	29.2	1.24 (2H, m)	28.5 <sup>a</sup>	1.25 (2H, m) 28.6 <sup>a</sup>
7	1.32 (2H, m)	25.1	1.26 (2H, m)	24.7	1.26 (2H, m) 24.5
8	1.53 (2H, m)	36.8	1.37 (2H, m)	36.3	1.49 (1H, m) 36.4 1.34 (1H, m)
9	4.20 (1H, m)	72.0	4.03 (1H, m)	69.8	4.35 (1H, m) 68.5
10	6.34 (1H, dd, <i>J</i> = 15.9, 5.7 Hz)	150.2	6.39 (1H, dd, <i>J</i> = 15.8, 5.1 Hz)	152.5	6.10 (1H, dd, <i>J</i> = 11.1, 8.7 Hz) 152.5
11	5.76 (1H, ddd, <i>J</i> = 15.9, 1.6, 0.8 Hz)	107.9	5.77 (1H, d, <i>J</i> = 15.8 Hz)	105.9	5.66 (1H, d, <i>J</i> = 11.1 Hz) 106.2
12		77.7		76.9	77.1
13		73.5		73.1	75.2
14		71.5		67.6	68.4
15		77.2		85.3	84.2
16	5.96 (1H, dq, <i>J</i> = 5.8, 0.8 Hz)	64.7	4.28 (1H, t, <i>J</i> = 6.5 Hz)	62.0	4.93 (1H, d, <i>J</i> = 5.4 Hz) 61.7
17	5.88 (1H, ddd, <i>J</i> = 16.9, 10.3, 5.7 Hz)	132.1	1.58 (2H, m)	30.3	5.88 (1H, ddd, <i>J</i> = 17.0, 10.1, 5.4 Hz) 137.3
18	<i>trans</i> : 5.55 (1H, dt, <i>J</i> = 16.9, 1.1 Hz) <i>cis</i> : 5.35 (1H, dt, <i>J</i> = 10.3, 1.1 Hz)	119.6	0.90 (3H, t, <i>J</i> = 7.4 Hz)	9.4	<i>trans</i> : 5.33 (1H, dt, <i>J</i> = 17.1, 1.5 Hz) <i>cis</i> : 5.16 (1H, dt, <i>J</i> = 10.1, 1.5 Hz) 115.5
1-OCH <sub>3</sub>	3.67 (3H, s)	51.5	3.58 (3H, s)	51.1	3.58 (3H, s) 51.0
16-OCOC		169.5			
H <sub>3</sub>					
16-OCOC	2.11 (3H, s)	20.9			
H <sub>3</sub>					

Assignments in the same column are interchangeable.suggesting that the olefinic protons were in the *E* configuration (Figure 3). Careful comparison of the 1D and 2D NMR spectra of **2** with those of **5** revealed similarities as a polyacetylene [37]. A major difference between **2** and **5** was the presence of an acetoxy group (δ<sub>H</sub> 2.11 and δ<sub>C</sub> 169.5 and 20.9) in the former. The location of the acetoxy group was assigned to C-16, as evidenced by the HMBC correlations from H-16 (δ<sub>H</sub> 5.96) to 16-OCOCH<sub>3</sub> (δ<sub>C</sub> 169.5) and 16-OCOCH<sub>3</sub> (δ<sub>H</sub> 2.11) to 16-OCOCH<sub>3</sub>.



**Figure 2.** Key  $^1\text{H}$ - $^1\text{H}$  COSY and HMBC correlations in 1-4.**Figure 3.** Key  $^1\text{H}$ - $^1\text{H}$  NOESY correlations in 1-4.

The HRESIMS exhibited that the molecular formula of **3** is  $\text{C}_{19}\text{H}_{28}\text{O}_4$  due to a molecular ion peak at  $m/z$  338.3419  $[\text{M}+\text{NH}_4]^+$ . The  $^1\text{H}$  NMR and  $^{13}\text{C}$  NMR spectra of **3** (Table 2) were quite similar to those of **5**. Unlike **5**, **3** lacked signals for an olefinic group, with methylene ( $\delta_{\text{H}}$  1.58/ $\delta_{\text{C}}$  30.3, C-17) and methyl ( $\delta_{\text{H}}$  0.90/ $\delta_{\text{C}}$  9.4, C-18) groups observed instead. In addition, the presence of an ethyl group attached to the C-16 position was established by COSY correlations between H-16/H-17 and H-17/H-18, as well as HMBC correlations from H-18 to C-16 and H-18 to C-17 (Figure 2). The NOE correlation observed between H-9 and H-11 suggested an *E* configuration of the olefinic protons.

Compound **4** was obtained as a brown amorphous solid, with a molecular ion peak at  $m/z$  336.2172  $[\text{M}+\text{NH}_4]^+$  from the HRESIMS in agreement with the molecular formula  $\text{C}_{19}\text{H}_{26}\text{O}_4$ . Although thorough 1D and 2D NMR interpretation of **4** showed a planar structure similar to **5**, the coupling constant between H-10 ( $\delta_{\text{H}}$  6.10) and H-11 (5.66) was 11.1 Hz, indicating the double bond as a *Z* geometric configuration [61]. There was no clear NOE correlation between H-8/H-10 and H-9/H-11, suggesting that the olefinic group was in the *Z* configuration.

A previous study reported the use of Mosher's derivatization method and ECD calculations to determine the absolute stereochemistry of polyacetylene compounds [61]. Based on that study, the absolute stereochemistry of compounds **2**–**5** was determined. By comparing the ECD spectra with the calculated values, two possible configurations, "9R16R" and "9R16S," were identified. Because the ECD spectra had limitations in definitively determining the absolute configuration between those two possibilities, a DP4+ simulation was used for the final structural assignment. A DP4+ simulation compares the calculated NMR chemical shifts of candidate structures with experimental data to determine which structure best matches the experimental data and thereby assign the structural configuration [62]. DP4+ simulations provide advantages by preventing incorrect assignments and offering additional support for newly assigned structures, particularly when experimental data are uncertain [63].

We calculated the two possible diastereomers (9R16S and 9R16R) for each structure by using a conformational search and geometric optimization to determine their relative configurations. The diastereomer with the highest probability was then subjected to further ECD calculations to elucidate the absolute configuration. The ECD spectra of the enantiomers were automatically generated without additional calculations. The DP4+ prediction results indicate that **3**–**5** share the same relative configuration (9R16S) with high confidence (Tables S4–S12 and Figures S39–S44). **2**, on the other hand, exhibited the opposite relative configuration (9R16R) with a high probability (99%) (Tables S1–S3 and Figures S37–S38). The ECD calculations confirmed the absolute configurations of **3**–**5** as 9R16S and that of **2** as 9R16R (Figure 4).

The polyacetylene compounds from *D. morbifera* are composed of seventeen or eighteen carbons, each containing two alkyne and two alkene functional groups, including (3S)-falcariinol, (3S,8S)-falcariindiol, and (3S)-diynene [64], most of which usually exist in a *cis* form [64–67]. In this study, the alkene functional group at C-10 and C-11 are in the *trans* form, except in **4**. Although **5** has been isolated before, its absolute configuration was not determined [37]. Therefore, we analyzed the absolute configuration of **5** using ECD calculations and DP4+ simulations. Polyacetylenes have been discovered in various plants, including *Bupleurum chinense* [68], *Carthamus tinctorius* [69], and *Codonopsis pilosula* [70]. Polyacetylenes isolated from natural products exhibit a range of biological

properties, such as HIV reverse transcriptase inhibition and antibacterial activity [17–20]. Notably, C<sub>17</sub>- and C<sub>18</sub>-polyacetylenes have been reported to possess potential cytotoxic properties [17,20,71]. It has been also reported that polyacetylenes act as phytoalexins, protecting plants from diseases and external factors [72]. Additionally, in the ecological environment, they play a role in preventing barnacle larvae by causing biofouling [73].

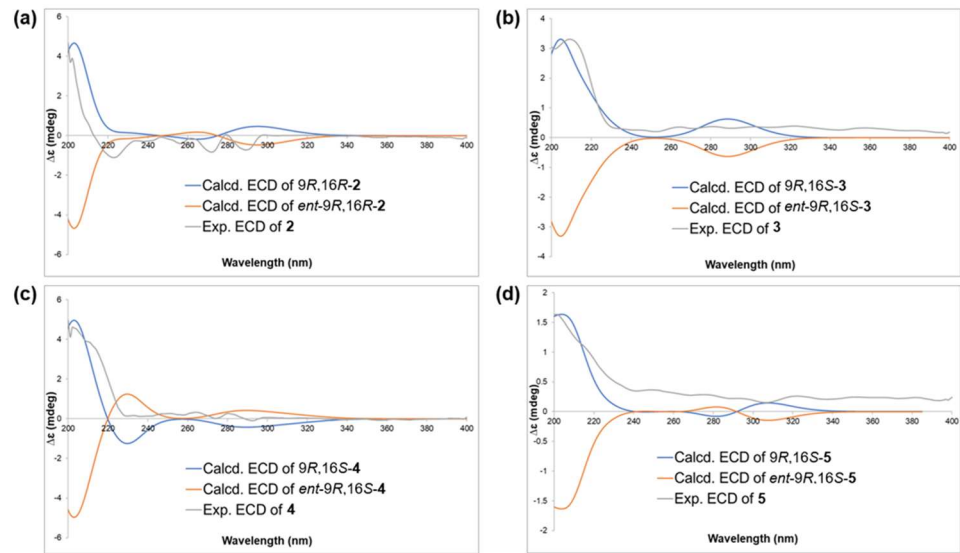


**Figure 4.** The ECD calculations of (a) 2, (b) 3, (c) 4, and (d) 5.

2.2. Molecular Docking

Molecular docking can be used to identify potential drugs for treating various diseases. To explore the potential effects of *D. morbifera* on metabolic syndromes, *in silico* docking simulations were conducted using compounds 1–11. These simulations aimed to examine the interactions and behavior of the compounds in AMPK and CTSS active sites. A control and compounds 1–11 were constructed in a 3D model, and molecular docking studies were conducted using four software programs (Autodock Vina, Autodock 4, LeDock, and Dock 6).

Among the compounds, 8 (-11.39 Kcal/mol) exhibited the highest affinity with AMPK, as shown in Table 3. Figure 5a and 5b show the molecular interaction models of 5-amino-4-imidazolecarboxamide ribonucleoside (AICAR, a well-known AMPK activator) and 8 with AMPK [74]. Although the control (AICAR) and 8 exhibit the same number of hydrogen bonds, 8 has a higher number of hydrophobic interactions, thereby demonstrating higher binding affinity. It is worth noting that both AICAR and 8 form the same hydrogen bond with the VAL96 residue, indicating that they are likely to have similar binding modes and thus related biological activities. This is the first study to conduct *in silico* simulations on compounds 1–11 with AMPK.

**Table 3.** Docking energy (Kcal/mol) of 1–11 and AICAR <sup>a</sup> with AMPK.

Compound	Autodock Vina	Autodock 4	LeDock	Dock 6
AICAR (Control)	-6.3	-7.4	-6.0	-33.5
1	-5.9	-6.1	-5.4	-55.3
2	-5.8	-5.3	-3.5	-42.9
3	-5.7	-5.3	-4.2	-38.3
4	-5.8	-5.8	-4.4	-39.5
5	-5.8	-5.5	-4.1	-35.6
6	-6.8	-7.2	-5.2	-37.8
7	-6.8	-8.7	-6.0	-55.5
8	-8.9	-11.4	-7.0	-40.6
9	-6.6	-6.6	-4.4	-46.3



10	-6.5	-9.3	-3.3	-28.5
11	-7.6	-7.9	-4.5	-43.8

<sup>a</sup> AICAR, 5-amino-4-imidazolecarboxamide ribonucleoside.

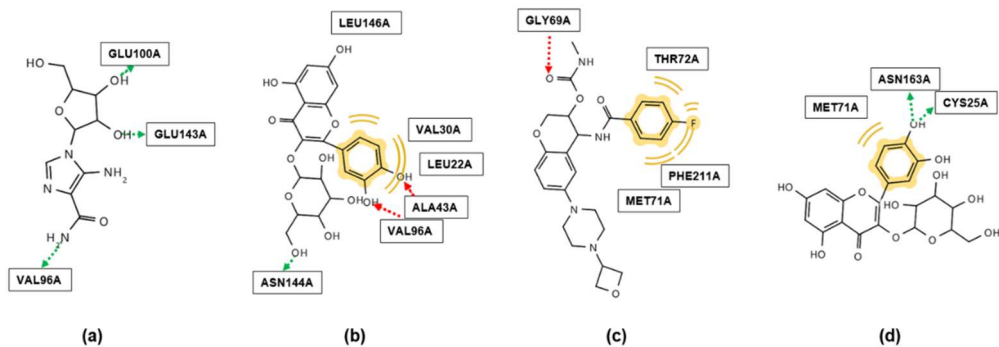


**Figure 5.** Binding interactions of (a) 5-amino-4-imidazolecarboxamide ribonucleoside (AICAR) and (b) **8** with AMP-activated protein kinase (AMPK) in *in silico* docking simulations in Autodock 4.2. The binding sites of (c) LY3000328 and (d) **8** with cathepsin S (CTSS) in docking simulations in Autodock 4.2. The green arrow indicates the hydrogen bond (H-bond) donor, the red arrow indicates the H-bond acceptor, and the yellow indicates hydrophobic interaction or van der Waals force. (ALA, Alanine; ASN, Asparagine; GLU, Glutamic acid; LEU, Leucine; VAL, Valine; ASN, Asparagine; CYS, Cysteine; GLY, Glycine; MET, Methionine; PHE, Phenylalanine; THR, Threonine).

Table 4 clearly shows that each compound exhibited various levels of binding affinity against CTSS. Especially in the case of compound **8**, it is evident that its affinity for the binding sites is more stable than that of the control and other compounds. Figure 5c and 5d exhibit the molecular interactions of **8** and LY3000328 (Z-FL-COCHO) against CTSS. The control provided hydrophobic/van der Waals interactions and acted as a hydrogen bond acceptor with CTSS (Figure 5c). As shown in Figure 5d, the B ring in **8** can form hydrophobic interactions/van der Waals forces, as well as hydrogen bonds with the CTSS receptor. To the best of our knowledge, this is the first study to conduct *in silico* simulations of compounds 1–11 against CTSS.

**Table 4.** Docking energy (Kcal/mol) of 1–11 and LY3000328 with CTSS.

Compound	Autodock Vina	Autodock 4	LeDock	Dock 6
LY3000328 (Control)	-7.2	-8.1	-5.6	-127.0
1	-6.1	-7.5	-5.5	-54.7
2	-5.2	-4.6	-4.0	-39.5
3	-5.7	-4.6	-4.2	-42.6
4	-5.7	-5.7	-4.5	-44.0
5	-5.6	-4.6	-4.2	-43.6
6	-6.3	-6.9	-5.8	-39.3
7	-6.5	-9.1	-5.8	-50.5
8	-8.1	-10.3	-6.1	-42.2
9	-6.5	-5.9	-4.5	-36.5
10	-8.5	-9.4	-3.8	-33.1
11	-6.9	-7.3	-4.6	-42.7

2.3. In Vitro Assay

To evaluate the results from the *in silico* simulations, *in vitro* AMPK assays were performed. Compound **8**, which showed the highest binding affinity with AMPK in the *in silico* simulation, increased the protein levels of AMPK, PPAR- $\alpha$ , and Sirt1 as a PPAR- $\alpha$  activator, as shown by a PPAR-

$\alpha$  luciferase assay (Figure 6a and 6b). Although a water extract and **8** were tested to investigate their inhibitory activity against CTSS, no positive result was observed.

Previous studies have demonstrated that a *D. morbifera* extract can activate AMPK and has therapeutic effects on diabetes, obesity, and nephrotoxicity [4,75,76]. Additionally, a patent suggests that it can enhance PPAR- $\alpha$  to regulate glucose activity [77]. Several studies have reported the biological effects of compounds **6** and **8** against AMPK. By regulating the AMPK pathway, **6** has showed potential to treat cardiac hypertrophy [78], diabetes [79], and obesity [80]. **8** can be applied to hypoxia-related diseases [81], particulate matter-induced lung injury [82], kidney function damage [83], and enhanced insulin resistance and lipid synthesis through the AMPK signaling pathway [84].

Although the *in vitro* CTSS-inhibition screening of **8** did not show positive effects, the attempt itself has important research value because it was the first attempt to evaluate the *in vitro* effects of **8** on CTSS.

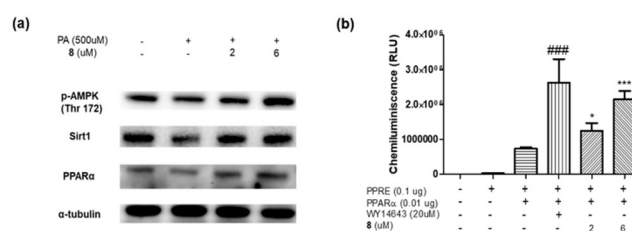


**Figure 6.** (a) The protein levels of AMPK, PPAR- $\alpha$ , and Sirt1 were measured in the presence of **8** using western blotting. (b) PPAR- $\alpha$  luciferase assay with **8**.

In this work, 11 compounds were isolated from *D. morbifera*: a new phenolic glucoside (**1**), three new polyacetynes (**2–4**), and 7 known compounds (**5–11**). Their structures were determined using 1D and 2D NMR spectroscopy and HRESIMS, and the absolute configurations of **2–5** were established through ECD calculations and DP4+ simulations. **5** is a known substance, but its absolute configuration had not been determined before this study. Although many phenolic glucosides have been identified in *D. morbifera*, such as gastrodin, nikoenoside, and isotachioside [85], the phenolic diglucoside (**1**) with a unique connectivity was here discovered for the first time. Based on a literature search to find therapeutic targets, all the isolated compounds were evaluated using *in silico* molecular docking to determine their binding affinity with AMPK and CTSS receptors. Among them, **8** exhibited the highest binding energy for both AMPK and CTSS. In the *in vitro* assays, **8** stimulated PPAR- $\alpha$  luciferase activity and increased the protein levels of AMPK, PPAR- $\alpha$ , and Sirt1, indicating its role as a PPAR- $\alpha$  activator. However, in the *in vitro* CTSS assays, **8** did not exhibit any significant inhibition of CTSS. Based on the biological activity of **8** as a PPAR- $\alpha$  activator, it can be inferred that **8** has potential for the treatment of diseases such as diabetes and obesity. Nevertheless, further research is needed to elucidate the specific mechanisms through which PPAR- $\alpha$  activation contributes to those diseases. This study expands our chemical and biological understanding of *D. morbifera* and will provide information to future investigators.

### 3. Materials and Methods

#### 3.1. Plant Materials

The leaves and stems of *Dendropanax morbifera* were collected at Tree Travel Botanical Garden in Hadong-gun, Gyeongsangnam-do, South Korea, in June 2021. A voucher specimen (No. EA391) was deposited at the Natural Product Chemistry Laboratory, College of Pharmacy, Ewha Womans University, Seoul, South Korea.

#### 3.2. General Experimental Procedures

Optical rotation was performed on a P-1010 polarimeter (Jasco, Tokyo, Japan), and the UV spectrum was recorded on a U-3000 spectrophotometer (Hitachi, Tokyo, Japan). NMR spectra were

acquired on a Varian Unity Inova 400 MHz FT-NMR instrument (Agilent Technologies, Santa Clara, CA, USA) with TMS as an internal standard, and the data were processed in MestReNova 9.0 (Mestrelab Research SL, Santiago de Compostela, Spain). HRESIMS was performed on an Agilent 6230 Accurate-Mass TOF LC/MS system (Agilent). CD measurements were performed using an Applied Photophysics Chirascan-Plus CD spectrometer (Applied Photophysics, Surrey, United Kingdom). For column chromatography, Diaion HP-20 and Kieselgel 60 F254 (silica gel, 0.25 mm layer thickness) were purchased from Mitsubishi Chemical Co. (Tokyo, Japan) and Merck & Co. (Rahway, NJ, USA), respectively. MPLC was performed using CombiFlash (Teledyne Isco Inc., Lincoln, NE, USA) equipped with a RediSep Rf C18 column (130 g, Teledyne Isco Inc.) and a RediSep Rf normal phase silica column (24 g and 40 g). Preparative HPLC purification was conducted using a Waters 600 pump and a Waters 996 photodiode array detector (Waters, Milford, MA, USA) equipped with a YMC-Pack Pro C18 column and a YMC Actus pro C18 column (5  $\mu$ m, 250 mm  $\times$  20 mm i.d., YMC Co., Kyoto, Japan).

### 3.3. Extraction and Isolation

The leaves and stems of *D. morbifera* (10 kg) were extracted with MeOH (3  $\times$  55 L) at room temperature for two days. The solvent was subjected to rotary evaporation to obtain a MeOH extract (1.6 kg). The extract was suspended in 2 L of distilled water and fractionated with hexanes (11  $\times$  2 L) and EtOAc (8  $\times$  2 L), yielding a hexane extract (207.5 g), EtOAc extract (126.7 g), and aqueous extract (2.5 L).

The EtOAc extract (126 g) was subjected to silica-gel column chromatography (CH<sub>2</sub>Cl<sub>2</sub>-MeOH, 1:0 to 0:1) to provide 15 fractions (A01–A15) and 8 (38 mg). Fractions A04 to A07 (25 g) were subjected to normal-phase column chromatography (hexane-EtOAc 0:1 to 1:0) to obtain 23 subfractions (A0401–A0423). Compound **10** (11 mg) was precipitated from subfraction A0402. Subfraction A0403 (162 mg) was separated by MPLC (hexane-EtOAc 1:0 to 0:1, 5 mL/min) to yield 14 subfractions (A040301–A040314). Subfraction A040302 (50 mg) was separated using silica gel (hexane-CH<sub>2</sub>Cl<sub>2</sub> 1:0 to 0:1) and applied to preparative HPLC (YMC-Park PRO C18, MeOH-water, 75:25, 3 mL/min) to acquire **2** (1 mg, *t<sub>r</sub>* 85 min). Subfraction A0408 (3.4 g) was subjected to MPLC (hexane-acetone, 1:0 to 0:1, 5 mL/min) to yield 15 subfractions (A040801–A040815). Subfraction A040804 (1.3 g) was chromatographed using silica gel (hexane-EtOAc, 1:0 to 0:1) to provide 19 subfractions (A04080401–A04080419). Compound **5** (7.5 mg, *t<sub>r</sub>* 52 min) was obtained from A04080416 (24 mg) by preparative HPLC (YMC-Park PRO C18, MeOH-water, 7:3, 4 mL/min). Subfraction A04080408 (694 mg) was separated by RP-18 (MeOH-water, 6:4 to 1:0) to provide 10 subfractions (A0408040801–A0408040810). Subfraction A0408040803 (37 mg) was subjected to preparative HPLC (YMC-Park PRO C18, MeOH-water, 65:35, 5 mL/min) to yield **3** (1 mg, *t<sub>r</sub>* 92 min). Subfraction A0415 (1.66 g) was subjected to MPLC (hexane-EtOAc 95:5 to 0:1) to yield **11** (100 mg). Subfraction A041508 (68 mg) was purified by preparative HPLC (YMC-Actus Triart C18, MeOH-H<sub>2</sub>O, 6:4, 4 mL/min) to obtain **4** (0.9 mg, *t<sub>r</sub>* 149 min).

#### *Morbiferoside A (1)*

Yellow amorphous solid;  $[\alpha]_D^{20} = -21.1$  (c 0.001, MeOH); UV (MeOH)  $\lambda_{\max}$ : 230, 284 nm; <sup>1</sup>H (methanol-*d*<sub>4</sub>, 400 MHz) and <sup>13</sup>C (methanol-*d*<sub>4</sub>, 100 MHz), NMR data, see Table 1; HRESIMS *m/z* 601.2136 [M + H]<sup>+</sup> (calculated for C<sub>27</sub>H<sub>37</sub>O<sub>15</sub>, 601.2134). 1-*O*- $\beta$ -[4-*O*-(3,5-dimethoxy-4-hydroxyphenyl)-glucopyranosyl]-2-methoxy-4-*C*- $\alpha$ -glucopyranoside.

#### *Methyl (10E,9R,16R)-16-acetoxy-9-hydroxyoctadeca-10,17-dien-12,14-diynoate (2)*

Brown amorphous solid;  $[\alpha]_D^{20} +3.3$  (c 0.001, CHCl<sub>3</sub>); UV (MeOH)  $\lambda_{\max}$ : 215, 254, 268, 284 nm; <sup>1</sup>H (chloroform-*d*, 400 MHz) and <sup>13</sup>C (chloroform-*d*, 100 MHz), NMR data, see Table 2; HRESIMS *m/z* 383.1835 [M + Na]<sup>+</sup> (calculated for C<sub>21</sub>H<sub>28</sub>O<sub>5</sub>Na, 383.1829).

#### *Methyl (10E,9R,16S)-9,16-dihydroxyoctadeca-10-en-12,14-diynoate (3)*

Brown amorphous solid;  $[\alpha]_D^{20}$   $-18.0$  (c 0.001, MeOH); UV (MeOH)  $\lambda_{\max}$ : 215, 254, 268, 283 nm;  $^1\text{H}$  (DMSO- $d_6$ , 400 MHz) and  $^{13}\text{C}$  (DMSO- $d_6$ , 100 MHz), NMR data, see Table 2; HRESIMS  $m/z$  338.3419  $[\text{M} + \text{NH}_4]^+$  (calculated for  $\text{C}_{19}\text{H}_{28}\text{O}_4\text{NH}_4$ , 338.3419).

#### *Methyl (10Z,9R,16S)-9,16-dihydroxyoctadeca-10,17-dien-12,14-diynoate (4)*

Brown amorphous solid;  $[\alpha]_D^{20}$   $-18.2$  (c 0.001, MeOH); UV (MeOH)  $\lambda_{\max}$ : 215, 254, 268, 283 nm;  $^1\text{H}$  (DMSO- $d_6$ , 400 MHz) and  $^{13}\text{C}$  (DMSO- $d_6$ , 100 MHz), NMR data, see Table 2; HRESIMS  $m/z$  336.2172  $[\text{M} + \text{NH}_4]^+$  (calculated for  $\text{C}_{19}\text{H}_{26}\text{O}_4\text{NH}_4$ , 336.217).

### 3.4. Conformational Search and DP4+ Calculation for 2–5

Conformational searches for **2–5** were performed using MacroModel (version 11.9, Schrödinger LLC, New York, USA) interfaced with Maestro (version 11.5, Schrödinger LLC) in a Merck molecular force field (MMFF94) in the gas phase. The conformers of **2**, **3**, and **5** were further geometrically optimized via density functional theory calculations made using TmoleX 4.3.2 and Turbomole 7.2 (COSMOLogic GmbH, Leverkusen, Germany) at the B3-LYP/def-SV(P) level in the gas phase, and the conformers of **4** were calculated at the CAM-B3LYP/def-SV(P) level. Optimized stable conformers with a Boltzmann population  $> 1\%$  were selected for NMR chemical shift calculation with the basis set at 6–311G(d,p) and the B3LYP functional level in the gas phase. The calculated isotropic magnetic shielding constants ( $\sigma$ ) were Boltzmann distribution averaged according to their free energies. The results were then put into Sarotti's Excel spreadsheet for calculation of the DP4+ probability to determine the best fit [86].

### 3.5. ECD Calculation

All conformers were geometrically optimized at the B3-LYP/def-SV(P) level in the gas phase. Stable conformers with a Boltzmann population of  $> 1\%$  were selected for the ECD calculation. ECD spectra were simulated using the TD-DFT method and applying the B3LYP/def-SVP level in the gas phase. The overall ECD curves were all weighted by the Boltzmann distribution and produced by SpecDis 1.71 software with a sigma/gamma value of 0.24 eV and UV corrections of  $-18$  nm (**2**),  $-10$  nm (**3**),  $-15$  nm (**4**), and  $-15$  nm (**5**) to facilitate comparison with the experimental data [87].

### 3.6. Molecular Docking

The crystal structures of AMPK and CTSS were obtained from the RCSB PDB website [PDB ID: 2Y94 (AMPK) and 6YYR (CTSS)] (<https://www.rcsb.org/>, accessed on 1 March 2024). The 3D structures of AICAR and LY3000328 were acquired from the PubChem website (<https://pubchem.ncbi.nlm.nih.gov/>, accessed on 1 March 2024). Four programs were used for the docking simulations: Autodock Vina 1.1.2 (<https://vina.scripps.edu/>, accessed on 1 March 2024), Autodock 4.2.6 (<https://autodock.scripps.edu/>, accessed on 1 March 2024), LeDock (<http://www.lephar.com/software.htm>, accessed on 1 March 2024), and Dock 6.10 ([https://www.dock.compbio.ucsf.edu/DOCK\\_6/](https://www.dock.compbio.ucsf.edu/DOCK_6/), accessed on 1 March 2024). Docking preparation was conducted to add hydrogens and assign charges to the compounds in UCSF Chimera (<https://www.rbvi.ucsf.edu/chimera/>, accessed on 1 March 2024). A pharmacophore analysis was conducted using LigandScout 4.0 (Inte:Ligand, Vienna, Austria, (<http://www.inteligand.com/ligandscout/>, accessed on 1 March 2024) to explore possible receptor and ligand interactions.

### 3.7. Cell Treatment Experiments

HepG2 cells (human liver cancer cell line) were purchased from the American Type Culture Collection (Manassas, VA, USA). The cells were cultured in Dulbecco's modified Eagle medium (Welgene, Gyeongsan, Gyeongsangbuk-do, Korea) supplemented with 10% heat-inactivated (56°C for 30 min) fetal bovine serum (Welgene), 100 U/mL penicillin, and 100  $\mu\text{g/mL}$  streptomycin (Welgene). The cells were maintained at 37°C in a humidified atmosphere with 5%  $\text{CO}_2$ . The medium

was replaced with fresh medium after 2 days to remove non-adherent cells or cell debris. To evaluate the effects of 8 on lipid accumulation, HepG2 cells were pretreated with 2.6  $\mu\text{M}$  8 for 3 h before treatment with BSA-conjugated palmitate (500  $\mu\text{M}$ ) for 24 h.

### 3.8. Protein Extraction and Western Blotting

To lyse the cells and extract proteins, the cells were rinsed with phosphate-buffered saline (PBS, Gibco, Grand Island, NY, USA) and collected using cold PBS. Total protein was extracted from the cells using cold RIPA buffer (Biosesang, Seongnam, Korea) containing a protease inhibitor cocktail (GenDEPOT, Katy, TX, USA) according to the manufacturer's protocol. Whole-cell lysates (10–40  $\mu\text{g}$  of protein) were prepared by heating at 98°C for 5 minutes in a gel-loading buffer (0.3125 M Tris-HCl pH 6.8, 2% SDS, 5% 2-mercaptoethanol, 0.05% bromophenol blue, and 25% glycerol) at a 4:1 volume ratio. Protein samples were quantified using Pierce™ BCA protein assay kits (Thermo Scientific, Waltham, MA, USA). The proteins were then separated using SDS-PAGE and transferred onto PVDF membranes (Millipore) with a Bio-Rad western system. The membranes were blocked for 45 minutes with 5% non-fat milk in TBS (50 mM Tris, 150 mM NaCl, pH 7.6) containing 0.1% Tween 20 (TBS-T). After blocking, the membranes were washed five times with TBS-T for 15 minutes each and incubated overnight at 4°C with primary antibodies at dilutions of 1:1,000. The next day, the membranes were washed four times with TBS-T for 15 minutes each and then incubated for 1 hour at 25°C with horseradish peroxidase (HRP)-conjugated secondary antibodies (1:10,000). The immunoblots were visualized using chemiluminescent HRP substrate (Advansta, San Jose, CA, USA) and a Davinchchemi CAS-400 (Davinch-K, Seoul, Korea), according to the manufacturer's instructions.

### 3.9. Transfection and Luciferase Assay

To examine the activity of 8 in cells, PPAR- $\alpha$  luciferase assays were performed. Twenty-four hours after transfection with Lipofectamine 3000 transfection reagent (Invitrogen, Grand Island, NY, USA) and a PPAR- $\alpha$  promoter-LUC plasmid (0.1  $\mu\text{g}$ ), cells were treated with 8 (2.6  $\mu\text{M}$ ) and WY14643 (20  $\mu\text{M}$ ) for 24 h. Luciferase activity was then detected using a One-Glo luciferase assay system (Promega, Madison, WI, USA) and measured using a luminometer (Berthold Technologies GmbH & Co., Bad Wildbad, Germany).

### 3.10. CTSS Activity Assay

The CTSS activity assay was performed as follows: Assay buffer was prepared from 50 mM potassium phosphate buffer (pH 6.5), 50 mM NaCl, 2 mM EDTA, 0.01% Triton X-100, and 0.5 mM DTT. To that buffer, 2  $\mu\text{L}$  of sample was added to meet 100  $\mu\text{L}$  of total solution. Subsequently, 20  $\mu\text{M}$  Z-VVR-AMC (Chinese Peptide Company, Hangzhou, China) was added as the CTSS substrate. The reaction was monitored kinetically for 30 minutes, with fluorescence measurements taken at an excitation wavelength of 380 nm and an emission wavelength of 460 nm.

### 3.11. Reagents

All antibodies were purchased from Santa Cruz Biotechnology (Dallas, TX, USA), Abcam (Cambridge, MA, USA), or Cell Signaling Technology, Inc. (Beverly, MA, USA). The primary antibodies were as follows: anti-PPAR- $\alpha$  (sc-398394), anti-Sirt1 (ab13749), anti- $\alpha$ -tubulin (sc-5286), and anti-AMPK (Thr172) (#2535). Palmitic acid (P9767) was obtained from Sigma-Aldrich (Milwaukee, WI, USA). WY14643, a PPAR- $\alpha$  agonist, was purchased from MedChemExpress (Monmouth Junction, NJ, USA).

**Supplementary Materials:** The supporting information can be downloaded at: [www.mdpi.com/xxx/s1](http://www.mdpi.com/xxx/s1).

**Author Contributions:** Conceptualization, D.P., H.Y.C., and E.K.S.; formal analysis, S.G.N.; investigation, D.P., I.Y., and H.W.K.; writing—original draft preparation, D.P. and I.Y.; writing—review and editing, D.P., I.Y., and E.K.S.; visualization, D.P., and I.Y.; supervision, H.Y.C and E.K.S.; funding acquisition, I.Y. and E.K.S. All authors have read and agreed to the published version of the manuscript.



**Funding:** This work was supported by a National Research Foundation of Korea (NRF) grant funded by the Korean government (MIST) (No. 2021R1A2C1003350). This research was also supported by the Basic Science Research Program through the National Research Foundation of Korea (NRF) funded by the Ministry of Education (RS-2023-00243759).

**Data Availability Statement:** Data will be made available on request.

**Acknowledgments:** The authors would like to thank the Ewha Drug Development Research Core Center for letting use Agilent 6230 TOF LC/MS instrument (Agilent, Santa Clara, CA, USA) and 400 MHz NMR spectrometer (AVANCE NEO Nanobay 400 MHz NMR Spectrometer, Bruker Switzerland AG, Fällanden, Switzerland).

**Conflicts of Interest:** The authors declare no conflicts of interest.

## References

1. Han, S.H.; Jung, Y.H.; Oh, M.H.; Ko, M.H.; Oh, Y.S.; Koh, S.C.; Kim, M.H.; Oh, M.Y. Phylogenetic relationship of the *Dendropanax morfer* and *D. trifidus* based on PCR-RAPD. *Korean J. Genet.* **1998**, *20*, 173–181.
2. Awais, M.; Akter, R.; Boopathi, V.; Ahn, J.C.; Lee, J.H.; Mathiyalagan, R.; Kwak, G.-Y.; Rauf, M.; Yang, D.C.; Lee, G.S.; et al. Discrimination of *Dendropanax morbifer* via HPLC fingerprinting and SNP analysis and its impact on obesity by modulating adipogenesis- and thermogenesis-related genes. *Front. Nutr.* **2023**, *10*, 1168095.
3. Bae, K. *The medicinal plants of Korea*; Kyo-Hak Publishing Company: Seoul, 2000; Volume 260.
4. Heo, M.-G.; Byun, J.-H.; Kim, J.; Choung, S.-Y. Treatment of *Dendropanax morbifer* leaves extract improves diabetic phenotype and inhibits diabetes induced retinal degeneration in db/db mice. *J. Funct. Foods* **2018**, *46*, 136–146.
5. Sun, S.; Li, T.; Jin, L.; Piao, Z.H.; Liu, B.; Ryu, Y.; Choi, S.Y.; Kim, G.R.; Jeong, J.E.; Wi, A.J.; et al. *Dendropanax morbifer* prevents cardiomyocyte hypertrophy by inhibiting the Sp1/GATA4 pathway. *Am. J. Chin. Med.* **2018**, *46*, 1021–1044.
6. Ko, Y.-C.; Liu, R.; Sun, H.-N.; Yun, B.-S.; Choi, H.S.; Lee, D.-S. Dihydroconiferyl ferulate isolated from *Dendropanax morbifer* H.Lév. suppresses stemness of breast cancer cells via nuclear EGFR/c-Myc signaling. *Pharmaceuticals* **2022**, *15*, 664.
7. Lee, J.-W.; Ryu, H.W.; Lee, S.U.; Son, T.H.; Park, H.A.; Kim, M.O.; Yuk, H.J.; Ahn, K.-S.; Oh, S.-R. Protective effect of polyacetylene from *Dendropanax morbifer* Leveille leaves on pulmonary inflammation induced by cigarette smoke and lipopolysaccharide. *J. Funct. Foods* **2017**, *32*, 358–366.
8. Balakrishnan, R.; Cho, D.-Y.; Su-Kim, I.; Choi, D.-K. *Dendropanax Morbiferus* and other species from the genus dendropanax: Therapeutic potential of its traditional uses, phytochemistry, and pharmacology. *Antioxidants* **2020**, *9*, 962.
9. Vogt, T. Phenylpropanoid biosynthesis. *Mol. Plant.* **2010**, *3*, 2–20.
10. Carvalho, A.A.; Andrade, L.N.; de Sousa, É, B.; de Sousa, D.P. Antitumor phenylpropanoids found in essential oils. *Biomed. Res. Int.* **2015**, *2015*, 392674.
11. Korkina, L.G. Phenylpropanoids as naturally occurring antioxidants: From plant defense to human health. *Cell. Mol. Biol.* **2007**, *53*, 15–25.
12. Korkina, L.; Kostyuk, V.; De Luca, C.; Pastore, S. Plant phenylpropanoids as emerging anti-inflammatory agents. *Mini-Rev. Med. Chem.* **2011**, *11*, 823–835.
13. Nabavi, S.M.; Šamec, D.; Tomczyk, M.; Milella, L.; Russo, D.; Habtemariam, S.; Suntar, I.; Rastrelli, L.; Daglia, M.; Xiao, J.; et al. Flavonoid biosynthetic pathways in plants: Versatile targets for metabolic engineering. *Biotechnol. Adv.* **2020**, *38*, 107316.
14. Rajasekar, M.; Bhuvanesh, P.; Varada, P.; Selvam, M. Review on anticancer activity of flavonoid derivatives: Recent developments and future perspectives. *Results Chem.* **2023**, *6*, 101059.
15. Ciumărnean, L.; Milaciu, M.V.; Runcan, O.; Vesa, Ș. C.; Răchișan, A.L.; Negrean, V.; Perné, M.G.; Donca, V.I.; Alexescu, T.G.; Para, I.; et al. The effects of flavonoids in cardiovascular diseases. *Molecules* **2020**, *25*, 4320.
16. Gouveia, H.; Urquiza-Martínez, M.V.; Manhães-de-Castro, R.; Costa-de-Santana, B.J.R.; Villarreal, J.P.; Mercado-Camargo, R.; Torner, L.; de Souza Aquino, J.; Toscano, A.E.; Guzmán-Quevedo, O. Effects of the treatment with flavonoids on metabolic syndrome components in humans: A systematic review focusing on mechanisms of action. *Int. J. Mol. Sci.* **2022**, *23*, 8344.
17. Minto, R.E.; Blacklock, B.J. Biosynthesis and function of polyacetylenes and allied natural products. *Prog. Lipid. Res.* **2008**, *47*, 233–306.
18. Christensen, L.P. *Biological activities of naturally occurring acetylenes and related compounds from higher plants*; Trivandrum, India: 1998; Volume 2, pp. 227–257.

19. Santos, J.A.M.; Santos, C.; Freitas Filho, J.R.; Menezes, P.H.; Freitas, J.C.R. Polyacetylene glycosides: Isolation, biological activities and synthesis. *Chem. Rec.* **2022**, *22*, e202100176.
20. Christensen, L.P.; Brandt, K. Bioactive polyacetylenes in food plants of the Apiaceae family: Occurrence, bioactivity and analysis. *J. Pharm. Biomed. Anal.* **2006**, *41*, 683-693.
21. Saklayen, M.G. The global epidemic of the metabolic syndrome. *Curr. Hypertens. Rep.* **2018**, *20*, 12.
22. Lim, S.; Eckel, R.H. Pharmacological treatment and therapeutic perspectives of metabolic syndrome. *Rev. Endocr. Metab. Disord.* **2014**, *15*, 329-341.
23. Diradourian, C.; Girard, J.; Pégorier, J.-P. Phosphorylation of PPARs: From molecular characterization to physiological relevance. *Biochimie* **2005**, *87*, 33-38.
24. Yoon, M. The role of PPAR $\alpha$  in lipid metabolism and obesity: Focusing on the effects of estrogen on PPAR $\alpha$  actions. *Pharmacol. Res.* **2009**, *60*, 151-159.
25. Towler, M.C.; Hardie, D.G. AMP-activated protein kinase in metabolic control and insulin signaling. *Circ. Res.* **2007**, *100*, 328-341.
26. Wang, H.; Mao, X.; Du, M. Phytanic acid activates PPAR $\alpha$  to promote beige adipogenic differentiation of preadipocytes. *J. Nutr. Biochem.* **2019**, *67*, 201-211.
27. Chanda, D.; Lee, C.H.; Kim, Y.H.; Noh, J.R.; Kim, D.K.; Park, J.H.; Hwang, J.H.; Lee, M.R.; Jeong, K.H.; Lee, I.K.; et al. Fenofibrate differentially regulates plasminogen activator inhibitor-1 gene expression via adenosine monophosphate-activated protein kinase-dependent induction of orphan nuclear receptor small heterodimer partner. *Hepatology* **2009**, *50*, 880-892.
28. Roy, R.; Zhang, B.; Moses, M.A. Making the cut: Protease-mediated regulation of angiogenesis. *Exp. Cell Res.* **2006**, *312*, 608-622.
29. Wilkinson, R.D.A.; Williams, R.; Scott, C.J.; Burden, R.E. Cathepsin S: Therapeutic, diagnostic, and prognostic potential. *Biol. Chem.* **2015**, *396*, 867-882.
30. Hsing, L.C.; Kirk, E.A.; McMillen, T.S.; Hsiao, S.H.; Caldwell, M.; Houston, B.; Rudensky, A.Y.; LeBoeuf, R.C. Roles for cathepsins S, L, and B in insulinitis and diabetes in the NOD mouse. *J. Autoimmun.* **2010**, *34*, 96-104.
31. Taleb, S.; Lacasa, D.; Bastard, J.P.; Poitou, C.; Cancellio, R.; Pelloux, V.; Viguerie, N.; Benis, A.; Zucker, J.D.; Bouillot, J.L.; et al. Cathepsin S, a novel biomarker of adiposity: Relevance to atherogenesis. *FASEB J.* **2005**, *19*, 1540-1542.
32. Zheng, J.; Zhuang, H.; Zhang, T.; Wang, Y.; Ran, T.; He, J.; Han, N.; Duan, J. Cathepsin S inhibitor reduces high-fat-induced adipogenesis, inflammatory infiltration, and hepatic lipid accumulation in obese mice. *Ann. Transl. Med.* **2022**, *10*, 1172.
33. Fuchs, N.; Meta, M.; Schuppan, D.; Nuhn, L.; Schirmeister, T. Novel opportunities for Cathepsin S inhibitors in cancer immunotherapy by nanocarrier-mediated delivery. *Cells* **2020**, *9*, 2021.
34. Wang, H.; Jiang, H.; Cheng, X.W. Cathepsin S are involved in human carotid atherosclerotic disease progression, mainly by mediating phagosomes: Bioinformatics and *in vivo* and *vitro* experiments. *PeerJ* **2022**, *10*, e12846.
35. Lee, J. Peroxisome proliferator-activated receptor (PPAR)  $\alpha/\gamma$  agonist. *Korean J. Intern. Med.* **2014**, *87*, 19.
36. Junco, J.J.; Cho, J.; Mancha, A.; Malik, G.; Wei, S.J.; Kim, D.J.; Liang, H.; DiGiovanni, J.; Slaga, T.J. Role of AMPK and PPAR $\alpha$  in the anti-skin cancer effects of ursolic acid. *Mol. Carcinog.* **2018**, *57*, 1698-1706.
37. Park, J.U.; Yang, S.Y.; Guo, R.H.; Li, H.X.; Kim, Y.H.; Kim, Y.R. Anti-melanogenic effect of *Dendropanax morbiferus* and its active components via protein kinase A/cyclic adenosine monophosphate-responsive binding protein- and p38 mitogen-activated protein kinase-mediated microphthalmia-associated transcription factor downregulation. *Front. Pharmacol.* **2020**, *11*, 507.
38. Niwa, M.; Iwadare, Y.; Wu, Y.-C.; Hirata, Y. Two new phenylpropanoid glycosides from *Wikstroemia sikokiana*. *Chem. Pharm. Bull.* **1988**, *36*, 1158-1161.
39. Foo, L.Y.; Lu, Y.; Molan, A.L.; Woodfield, D.R.; McNabb, W.C. The phenols and prodelphinidins of white clover flowers. *Phytochemistry* **2000**, *54*, 539-548.
40. Achenbach, H.; Benirschke, G. Joannesialactone and other compounds from *Joannesia princeps*. *Phytochemistry* **1997**, *45*, 149-157.
41. Van Kiem, P.; Van Minh, C.; Huong, H.T.; Nam, N.H.; Lee, J.J.; Kim, Y.H. Pentacyclic triterpenoids from *Mallotus apelta*. *Arch. Pharm. Res.* **2004**, *27*, 1109-1113.
42. Ma, Z.Z.; Hano, Y.; Nomura, T.; Chen, Y.J. Alkaloids and phenylpropanoids from *Peganum nigellastrum*. *Phytochemistry* **2000**, *53*, 1075-1078.
43. Arshad, L.; Haque, M.A.; Harikrishnan, H.; Ibrahim, S.; Jantan, I. Syringin from *Tinospora crispa* downregulates pro-inflammatory mediator production through MyD88-dependent pathways in lipopolysaccharide (LPS)-induced U937 macrophages. *Mol. Biol. Rep.* **2024**, *51*, 789.
44. Aventurado, A.C.; Castillo, L.A.; Vasquez, D.R. Syringin as TGF- $\beta$ R1, HER2, EGFR, FGFR4 kinase, and MMP-2 inhibitor and potential cytotoxic agent against ER+ breast cancer cells. *Curr. Enzyme Inhib.* **2023**, *19*, 55-64.

45. Singh, V.K.; Thakur, D.C.; Rajak, N.; Giri, R.; Garg, N. Immunomodulatory potential of bioactive glycoside syringin: A network pharmacology and molecular modeling approach. *J. Biomol. Struct. Dyn.* **2023**, *42*, 3906-3919.
46. Gohari, A.; Saeidnia, S.; Bayati-Moghadam, M.; Amin, G.; Hadjiakhoondi, A. Phytochemical and chemotaxonomic investigation of *Stelleropsis iranica*. *Aust. J. Basic Appl. Sci.* **2009**, *3*, 3423-3427.
47. Ullah, N.; Ahmad, S.; Malik, A. Phenylpropanoid glycosides from *Daphne oleoides*. *Chem. Pharm. Bull.* **1999**, *47*, 114-115.
48. Jang, S.-A.; Park, D.W.; Sohn, E.H.; Lee, S.R.; Kang, S.C. Hyperoside suppresses tumor necrosis factor  $\alpha$ -mediated vascular inflammatory responses by downregulating mitogen-activated protein kinases and nuclear factor- $\kappa$ B signaling. *Chem.-Biol. Interact.* **2018**, *294*, 48-55.
49. Orzelska-Górka, J.; Szweczyk, K.; Gawrońska-Grzywacz, M.; Kędzierska, E.; Głowacka, E.; Herbet, M.; Dudka, J.; Biała, G. Monoaminergic system is implicated in the antidepressant-like effect of hyperoside and protocatechuic acid isolated from *Impatiens glandulifera* Royle in mice. *Neurochem. Int.* **2019**, *128*, 206-214.
50. Sun, Y.; Sun, F.; Feng, W.; Qiu, X.; Liu, Y.; Yang, B.; Chen, Y.; Xia, P. Hyperoside inhibits biofilm formation of *Pseudomonas aeruginosa*. *Exp. Ther. Med.* **2017**, *14*, 1647-1652.
51. Li, S.C.; Jin, Y.J.; Xue, X.; Li, J.; Xu, G.H. Chemical constituents from the bark of *Betula platyphylla*. *Chem. Nat. Compd.* **2023**, *59*, 190-192.
52. Voravuthikunchai, S.P.; Kanchanapoom, T.; Sawangjaroen, N.; Hutadilok-Towatana, N. Antioxidant, antibacterial and antiangiogenic activities of *Walsura robusta* Roxb. *Nat. Prod. Res.* **2010**, *24*, 813-824.
53. Ren, X.; Yun, X.; Yang, T.; Xu, T.; Shi, D.; Li, X. Epifriedelanol delays the aging of porcine oocytes matured *in vitro*. *Toxicol.* **2023**, *233*, 107256.
54. Kundu, J.K.; Rouf, A.S.S.; Nazmul Hossain, M.; Hasan, C.M.; Rashid, M.A. Antitumor activity of epifriedelanol from *Vitis trifolia*. *Fitoterapia* **2000**, *71*, 577-579.
55. Msengwa, Z.; Rwegoshora, F.; Credo, D.; Mwesongo, J.; Mafuru, M.; Mabiki, F.; John Mwang'onde, B.; Mtambo, M.; Kusiluka, L.; Mdegela, R.; et al. Epifriedelanol is the key compound to antibacterial effects of extracts of *Synadenium glaucescens* (Pax) against medically important bacteria. *Front. Trop. Dis.* **2023**, *3*, 107256.
56. Wu, L.-Z.; Wu, H.-F.; Xu, X.-D.; Yang, J.-S. Two new flavone C-glycosides from *Trollius ledebourii*. *Chem. Pharm. Bull.* **2011**, *59*, 1393-1395.
57. Wen, H.; Chen, C.; Sun, W.; Zang, Y.; Li, Q.; Wang, W.; Zeng, F.; Liu, J.; Zhou, Y.; Zhou, Q.; et al. Phenolic C-glycosides and aglycones from marine-derived *Aspergillus* sp. and their anti-inflammatory activities. *J. Nat. Prod.* **2019**, *82*, 1098-1106.
58. Roslund, M.U.; Tähtinen, P.; Niemitz, M.; Sjöholm, R. Complete assignments of the  $^1\text{H}$  and  $^{13}\text{C}$  chemical shifts and  $J_{\text{H-H}}$  coupling constants in NMR spectra of D-glucopyranose and all D-glucopyranosyl-d-glucopyranosides. *Carbohydr. Res.* **2008**, *343*, 101-112.
59. Fujimatu, E.; Ishikawa, T.; Kitajima, J. Aromatic compound glucosides, alkyl glucoside and glucide from the fruit of anise. *Phytochemistry* **2003**, *63*, 609-616.
60. Ryu, B.; Park, E.-J.; Doan, T.-P.; Cho, H.-M.; An, J.-P.; Pham, T.-L.-G.; Pham, H.-T.-T.; Oh, W.-K. Heliciopsides A-E, unusual macrocyclic and phenolic glycosides from the leaves of *Heliciopsis terminalis* and their stimulation of glucose uptake. *Pharmaceuticals* **2022**, *15*, 1315.
61. Xu, W.J.; Li, J.H.; Zhou, M.M.; Luo, J.; Jian, K.L.; Tian, X.M.; Xia, Y.Z.; Yang, L.; Luo, J.; Kong, L.Y. Toonasindiynes A-F, new polyacetylenes from *Toona sinensis* with cytotoxic and anti-inflammatory activities. *Fitoterapia* **2020**, *146*, 104667.
62. Smith, S.G.; Goodman, J.M. Assigning stereochemistry to single diastereoisomers by GIAO NMR calculation: The DP4 probability. *J. Am. Chem. Soc.* **2010**, *132*, 12946-12959.
63. Marcarino, M.O.; Cicetti, S.; Zanardi, M.M.; Sarotti, A.M. A critical review on the use of DP4+ in the structural elucidation of natural products: The good, the bad and the ugly. A practical guide. *Nat. Prod. Rep.* **2022**, *39*, 58-76.
64. Chung, I.-M.; Song, H.-K.; Kim, S.-J.; Moon, H.-I. Anticomplement activity of polyacetylenes from leaves of *Dendropanax moribifera* Leveille. *Phytother. Res.* **2011**, *25*, 784-786.
65. Park, B.-Y.; Min, B.-S.; Oh, S.-R.; Kim, J.-H.; Kim, T.-J.; Kim, D.-H.; Bae, K.-H.; Lee, H.-K. Isolation and anticomplement activity of compounds from *Dendropanax moribifera*. *J. Ethnopharmacol.* **2004**, *90*, 403-408.
66. Kim, E.H.; Jo, C.S.; Ryu, S.Y.; Kim, S.H.; Lee, J.Y. Anti-osteoclastogenic diacetylenic components of *Dendropanax moribifera*. *Arch. Pharm. Res.* **2018**, *41*, 506-512.
67. Kim, M.-O.; Kang, M.-J.; Lee, S.-U.; Kim, D.-Y.; Jang, H.-J.; An, J.H.; Lee, H.-S.; Ryu, H.W.; Oh, S.-R. Polyacetylene (9Z,16S)-16-hydroxy-9,17-octadecadiene-12,14-dienoic acid in *Dendropanax moribifera* leaves. *Food Biosci.* **2021**, *40*, 100878.
68. Cao, T.Q.; Vu, N.K.; Woo, M.H.; Min, B.S. New polyacetylene and other compounds from *Bupleurum chinense* and their chemotaxonomic significance. *Biochem. Syst. Ecol.* **2020**, *92*, 104090.
69. Baek, S.C.; Yi, S.A.; Lee, B.S.; Yu, J.S.; Kim, J.-C.; Pang, C.; Jang, T.S.; Lee, J.; Kim, K.H. Anti-adipogenic polyacetylene glycosides from the florets of safflower (*Carthamus tinctorius*). *Biomedicines* **2021**, *9*, 91.

**Disclaimer/Publisher's Note:** The statements, opinions and data contained in all publications are solely those of the individual author(s) and contributor(s) and not of MDPI and/or the editor(s). MDPI and/or the editor(s) disclaim responsibility for any injury to people or property resulting from any ideas, methods, instructions or products referred to in the content.